Particuology 115 (2026) 148–156

Contents lists available at ScienceDirect

Particuology

journal homepage: www.elsevier.com/locate/partic

Numerical modelling of reaction behavior for chemical looping hydrogen production system by CPFD

Liyan Sun[a,b,*], Yuedong Zhang[a], Jialei Cao[a], Rui Xiao[a]

[a] Key Laboratory of Energy Thermal Conversion and Control of Ministry of Education, School of Energy and Environment, Southeast University, Nanjing, 211189, China
[b] Xinjiang Key Laboratory of High Value Green Utilization of Low-rank Coal, Changji, 831100, China

HIGHLIGHTS

- Numerical simulation of a full-cycle chemical looping hydrogen production system is carried out.
- Inter-reactor cycling characteristics and microscopic details were investigated.
- Results validated the feasibility of CLHP and established references for advancing CLHP.

GRAPHICAL ABSTRACT

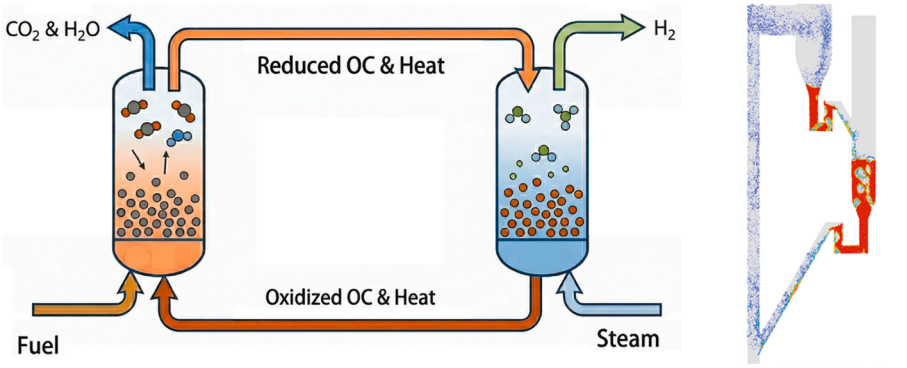

Schematic diagram and simulated structure of hydrogen production via chemical looping

ARTICLE INFO

Keywords:
Chemical looping hydrogen production
Numerical simulation
CPFD
Reaction behavior

ABSTRACT

Hydrogen stands as a pivotal energy carrier with significant potential to facilitate the global transition towards a low-carbon energy future. The main challenge in current stage is the production of hydrogen with less emission and high efficiency. To resolve this problem, chemical looping hydrogen production (CLHP) is proposed and investigated. The key factors influencing the efficiency of CLHP are the gas-solid flow, heat transfer and mass transfer processes. A dual-reactor system is established in this work and numerical model based on CPFD is utilised for investigating the reaction characteristics. Hydrogen production decreases with increasing gas velocity in the hydrogen production reactor. Variations in the solid circulation rate alter the mass and heat distribution within the system, consequently affecting the hydrogen production rate. A riser gas velocity of 7 m/s and a circulation rate of 0.15 kg/s are the recommended values for the current constructor. Overall, reactor temperature remains the predominant influencing factor. This study provides insights for reactor optimization and scale-up design.

* Corresponding author. Key Laboratory of Energy Thermal Conversion and Control of Ministry of Education, School of Energy and Environment, Southeast University, Nanjing, 211189, China.
E-mail address: sunliyan@seu.edu.cn (L. Sun).

https://doi.org/10.1016/j.partic.2026.04.010
Received 22 January 2026; Received in revised form 4 April 2026; Accepted 13 April 2026
Available online 27 April 2026

1. Introduction

Hydrogen stands as a pivotal energy carrier with potential to facilitate the global transition towards a low-carbon energy future (Wang et al., 2020). Combined with biomass utilization, this enables a technical pathway for hydrogen production with carbon neutrality (Duan et al., 2025). However, the environmental benefits of hydrogen utilization are critically dependent on the production method. Currently, the majority of hydrogen supply is derived from fossil fuels, primarily through steam methane reforming (SMR) and coal gasification (Yin et al., 2025). This creates a fundamental contradiction, the pursuit of a clean energy carrier is undermined by the carbon-intensive nature of its dominant production ways. The increasing demand for hydrogen contribute to a challenge to sustainability and less-emission (Uddin et al., 2025).

Among the emerging alternatives, chemical looping hydrogen production (CLHP) has garnered considerable attention as a highly promising and efficient approach. CLHP employs a solid oxygen carrier to indirectly transfer oxygen from an oxidant to the fuel source, as shown in Fig. 1. The development of oxygen carriers (Das et al., 2022; Zhang et al., 2025; Zhao et al., 2021) and experimental research (Cao, Liu, et al., 2024; Xue et al., 2012) have validated the technical feasibility of the technology. To enhance the reaction activity of oxygen carriers, the efficiency of chemical looping hydrogen production can be improved to meet operational requirements by introducing external fields (Abdullah et al., 2024; Chen et al., 2025). Economic analysis of chemical looping hydrogen production technology also shows the distinct advantages (Chiesa et al., 2008). These studies give researchers more confidence in chemical looping technology.

Compared to conventional SMR with post-combustion capture, CLHP offers the key advantages of higher thermodynamic efficiency and substantially lower CO_2 emissions. By eliminating the need for direct fuel combustion and the subsequent energy-intensive gas separation steps, CLHP offers a pathway towards truly low-carbon. With the advancements in computational fluid dynamics (CFD), numerical simulations enable a better understanding of the operational mechanisms and reaction characteristics of chemical looping systems (Jin et al., 2025). Hamidouche et al. (2019, 2020) simulated the chemical looping combustion process in a circulation mode and botn hydrodynamic behavior and reactive behaviors were obtained and analysed. Sun et al. (2022, 2023) investigated the performance of 150 kW and 1 MW chemical looping system by numerical method and microscopic details were revealed. These works provide a novel research methodology and a micro perspective, while, reports on numerical simulations of CLHP systems have been scarcely reported in the literature to date. Further research is warranted to elucidate the micro-scale characteristics and operational mechanisms of chemical looping hydrogen generation, particularly the holistic system behavior throughout the entire process structure.

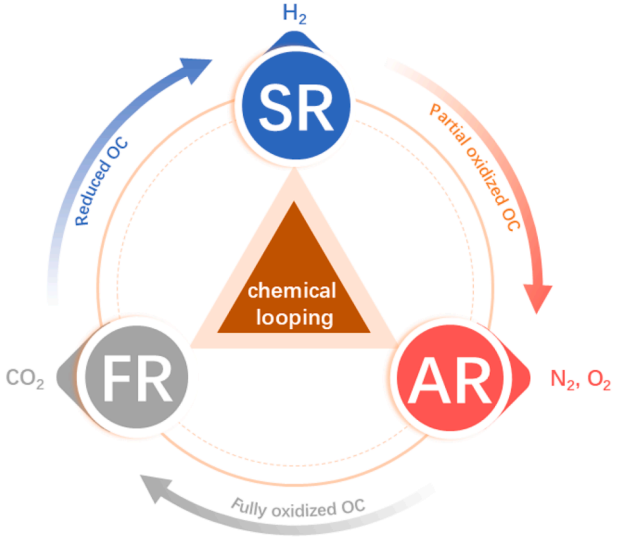

Fig. 1. Schematic diagram of chemical looping hydrogen production system. AR, FR and SR represent for air reactor, fuel reactor and steam reactor, respectively.

This work focused on investigating the reaction characteristics in CLHP system by numerical simulation. A CPFD model was utilised for optimizing CLHP efficiency and analyzing the feasibility of CLHP. A fully integrated CLHP system was constructed, comprising a fuel reactor, a steam reactor, a cyclone separator, and a loop seal (solids return system). The effects of oxygen carrier properties and operating conditions were evaluated which will be helpful for optimization and design. This work aims to contribute to the advancement of chemical looping hydrogen production technology through a comprehensive understanding of the underlying flow and reaction characteristics.

2. Computational particle fluid dynamics model

Computational particle fluid dynamics (CPFD) was adopted for simulating the chemical looping process, which is based on Euler-Lagrange model. Gas phase is regarded as a continuous medium and the motion of gas phase is described Navier-Stokes equations (Jiang et al., 2024). Considering the balance between accuracy and computational cost, large eddy simulation was used for modelling gas turbulence. Chemical reaction models and the boundary conditions and analysis methods in the numerical simulations were introduced as following (Li et al., 2020).

2.1. Governing equations for gas phase

Finite volume method is utilised for realizing the discretization the governing equations. And the mass conservation equation for per unit volume is written as following,

$$\frac{\partial(\epsilon_g\rho_g)}{\partial t}+\nabla(\epsilon_g\rho_g u_g)=\delta m_g \tag{1}$$

where ϵ_g, ρ_g and u_g are volume fraction of gas phase, density and velocity, respectively. δm_g represents the mass transfer rate per unit volume between gas phase and solid phase which is caused by chemical reactions.

Momentum conservation equation for gas phase is written as following,

$$\frac{\partial(\epsilon_g\rho_g u_g)}{\partial t}+\nabla(\epsilon_g\rho_g u_g u_g)=-\nabla P+F+\epsilon_g\rho_g\mathbf{g}+\nabla\epsilon_g\tau_g \tag{2}$$

where F is the interaction force between gas phase and solid phase, which is the domain factor influencing the accurate. τ_g is the stress tensor is defined as following,

$$\tau_g=\mu_g\left(\frac{\partial u_i}{\partial x_j}+\frac{\partial u_j}{\partial x_i}\right)-\frac{2}{3}\mu_g\delta_{ij}\frac{\partial u_k}{\partial x_k} \tag{3}$$

where μ_g is effective viscosity, $\mu_g=\mu_{gt}+\mu_{gl}$.

Species transportation equation is written as following,

$$\frac{(\epsilon_g\rho_g Y_i)}{\partial t}+\nabla\left((\epsilon_g\rho_g Y_i u_g\right)=\nabla\cdot\left(\rho_g D\epsilon_g\nabla Y_i\right)+\delta m_i \tag{4}$$

where Y_i is the mass fraction of each gas species and $\sum_{i=1}^{N}Y_i=1$ δm_i is the species mass changing caused by heterogeneous reactions.

Energy conservation equation for gas phase is shown as following,

$$\frac{\partial(\epsilon_g\rho_g h_g)}{\partial t}+\nabla\cdot(\epsilon_g\rho_g h_g u_g)=\epsilon_g\left(\frac{\partial p}{\partial t}+u_g\cdot\nabla p\right)+Q_{gs}+\delta m_g h_g \tag{5}$$

where Q_{gs} is energy source term and it is the energy caused due to reaction in this work. $\delta m_g h_g$ represents the energy source term due to the mass transfer.

Large eddy simulation method is utilised for

modelling the turbulent effect for gas phase. Large vortices with size larger than subgrid size ($\Delta = (\Delta x \Delta y \Delta z)^{1/3}$) are calculated from Navier-Stokes equation, while smaller one will be modelled by Smagorinsky model as following (Gupta et al., 2021; Wang et al., 2017),

$$\mu_{gt} = C\rho_g \Delta^2 \left| \frac{\partial u_i}{\partial x_j} + \frac{\partial u_j}{\partial x_i} \right| \tag{6}$$

where C is constant of Smagorinsky model which depends on the flow regime. Fort single phase flow, C ranges from 0.065 to 0.25. Chiesa et al. (2005) chosen 0.079 for simulating riser. In the work of Yin et al. (2010), the value was set equal to 0.12. And more details can be found in (Snider et al., 2011). With these assumptions, the effective viscosity can be calculated as,

$$\mu_g = \mu_{gt} + \mu_{gl} \tag{7}$$

2.2. Governing equations for solid particles

Particles' motion are obtained by solving transport equation according to Newton's second law (Chen et al., 2019). The difference for MP-PIC is that the particle distribution is solved as a function of spatial position, velocity, solid mass, temperature and time, $f_p(x, u, m, T, t)$. The transport of distribution density is written as following,

$$\frac{\partial f_p}{\partial t} + \frac{\partial (f_p u_p)}{\partial x} + \frac{\partial (f_p a_p)}{\partial u_p} = \frac{f_D - f_p}{\tau_D} \tag{8}$$

where τ_D is the relax time for collision. a_p is the particle acceleration,

$$a_p = F_D(u_g - u_p) - \frac{1}{\rho_p}\nabla p + g - \frac{1}{\epsilon_p \rho_p}\nabla \tau_p + \frac{u_p - u_g}{\tau_D} \tag{9}$$

where F_D is the interphase interaction and it is drag force for current work. And τ_S is calculated as following,

$$\tau_s = \frac{10 P_p \alpha_p^{\beta}}{max\left[(\epsilon_{cp} - \epsilon_p), \epsilon(1 - \epsilon_p)\right]} \tag{10}$$

where ϵ_{cp} is the maximum bulk density of solid, $\epsilon_{cp} = 0.63$.

2.3. Interphase interaction

For heterogeneous process, there are mass transfer, energy exchange and momentum transfer between gas and solid phase. We can find source term for continuity equation and energy equation. The last one, momentum transfer, is caused mainly by drag force between gas and solid phase. In this work, Gidaspow model is adopted to calculated drag coefficient, which is based on the difference of solid voidage (Prabhansu et al., 2015). The interaction force can be written as following (Zhu et al., 2023),

$$f_D = \frac{V_p \beta (\mathbf{u}_g - \mathbf{u}_s)}{1 - \epsilon_g} \tag{11}$$

The moment exchange coefficient, β, is written as following,

$$\beta = \begin{cases} 150\dfrac{\epsilon_p^2 \mu_g}{\epsilon_g d_p^2} + 1.75\dfrac{\epsilon_p \rho_g}{d_p}|\mathbf{u}_g - \mathbf{u}_p| & \epsilon_g < 0.8 \\ \dfrac{3}{4} C_D \dfrac{\epsilon_s \rho_g}{d_p}|\mathbf{u}_g - \mathbf{u}_p| \epsilon^{-1.65} & \epsilon_g \geq 0.8 \end{cases} \tag{12}$$

When the voidage is larger than 0.8, Ergun equation is used to calculate interphase momentum transportation, while, Wen-Yu model is adopted for case with voidage is smaller than 0.8. And C_D, drag coefficient, is calculated according to following equation,

$$C_D = \begin{cases} \dfrac{24g}{Re}\left[1 + 0.15\mathrm{Re}^{0.687}\right] & \mathrm{Re} < 1000 \\ 0.44 & \mathrm{Re} \geq 1000 \end{cases} \tag{13}$$

where Re represents Reynolds number,

$$\mathrm{Re} = \frac{\epsilon_g \rho_g d_p |u_g - u_p|}{\mu_g} \tag{14}$$

μ_g represents gas viscosity and d_p is particle diameter. Generally, the EMMS model can provide more accurate predictions of interphase interactions by accounting for mesoscale effects (Liu et al., 2011; Zhang et al., 2024). In this work, considering both computational accuracy and time consumption, the classical Gidaspow model is adopted.

2.4. Chemical reaction model

Oxygen carrier used in this work is Fe_3O_4/Al_2O_3 and was tested in our previous work (Gao et al., 2024). The fuel utilised is the mixture of CH_4, CO and H_2, which is similar to biomass gasification products. The heterogeneous reactions between reductive gases and oxygen carriers will lead to the mass exchange between phases. Shrinking-core model is used for calculating the mass changing rate (Abad et al., 2011),

$$\frac{t}{\tau} = 1 - (1 - X)^{1/3} \tag{15}$$

where $\tau = \frac{\rho_m r_g}{b k_s C_g^n}$ r_g is the grain size and n is reaction order. k_s is the reaction rate which is calculated according to Arrhenius' law,

$$k_s = k_0 \exp\left(-\frac{E}{RT}\right) \tag{16}$$

X is the reduction level of oxygen carrier, $X = \frac{m_o - m}{m_o - m_r}$, and the changing rate of reduction level is,

$$\frac{dX}{dt} = -\frac{1}{m_o - m_r}\frac{dm}{dt} \tag{17}$$

where m is the current mass of oxygen carrier. m_o and m_r are fully oxidized and fully reduced state mass of oxygen carrier, respectively. Then, the reduction rate with gases are calculated as following,

$$\dot{m}_{CO} = -(m_o - m_r)\frac{dX}{dt}\frac{2MW_{CO}}{MW_{O_2}} \tag{18}$$

$$\dot{m}_{CH_4} = -(m_o - m_r)\frac{dX}{dt}\frac{MW_{CH_4}}{2MW_{O_2}} \tag{19}$$

$$\dot{m}_{H_2} = -(m_o - m_r)\frac{dX}{dt}\frac{2MW_{H_2}}{MW_{O_2}} \tag{20}$$

The reaction rate with steam is calculated as following,

$$\frac{dX}{dt} = k_o exp\left(-\frac{E}{RT}\right) f(\alpha) C_g^n \tag{21}$$

where $f(\alpha)$ is the structure function of oxygen carrier, and mass change rate is

$$\dot{m}_{H_2O} = -(m_o - m_r)\frac{dX}{dt}\frac{2MW_{H_2O}}{MW_{O_2}} \tag{22}$$

The parameters for reaction of oxygen carrier are listed in Table 1.

Table 1
Chemical reaction kinetics parameters of CLHP.

Parameter	H_2	CO	CH_4	H_2O
ρ_m (mol/m^3)	11422	11422	11422	
r_g (m)	0.5×10^{-6}	0.5×10^{-6}	0.5×10^{-6}	
b	1.19	1.19	4.74	
k_0 (mol^{1-n}m^{3n-2}s^{-1})	0.51	0.21	8.8	65
E (kJ/mol)	109.2	113.3	165.2	103
n	1	1	1	0.5

2.5. Calculation conditions

The geometric model of reactor and inlets are built according to experimental structure (Cao, Sun, et al., 2024), as shown in Fig. 2. The inner diameter and height of riser are 0.1 m and 3.0 m, respectively. The inner diameter of fuel reactor is 0.2 m and the height is 1.7 m. Iron based oxygen carrier is selected due to its excellent chemical properties and thermodynamic stability (Yin et al., 2025). The size and density of oxygen carrier are 200 μm and 2650 kg/m^3, respectively. The outlets are set at the top of reactor which connect to atmosphere. Non-slip boundary condition is utilised for walls. Calculation parameters used in this work are listed in Table 2. In this work, four representative mesh sizes were selected: 15, 12, 10, and 8 mm. The solid-phase mass flow rate was used as a reference for grid independence verification, as shown in Fig. 3. The particle mass flow rate decreases with increasing mesh resolution, and remains relatively stable at mesh sizes of 10 and 8 mm. Considering both computational efficiency and accuracy, a mesh size of 10 mm was chosen for the simulations.

3. Results and discussion

3.1. Flow and reaction characteristics of CLHP

Fig. 4 shows the particle distribution pattern within the chemical looping system. Initially, particles are densely packed in the fuel reactor, cyclone and loop seals. As gas enters through the inlets, particle fluidization commences. Bubbles become visible within the fuel reactor, gradually rising and ultimately bursting at the surface. Driven by the fluidizing gas entering the riser, particles from the return leg are transported upwards. Particles exiting the top of the riser are then separated by the cyclone and returned to the fuel reactor. A completing cycle is achieved for oxygen carrier.Oxygen carriers circulate between fuel reactor and steam reactor and transfer lattice oxygen and heat, simultaneously. This is the most parameter which will further influence the reaction characteristics. Fig. 5 shows the solid circulating rate. Due to the interaction between bubbles and particles in the fluidized bed system, the solid phase flow becomes unstable, and the particle circulation volume fluctuates continuously over time. Time-averaged circulating rate is 0.11 kg/s under current conditions.

Pressure serves as the most critical parameter in fluidized bed reactors. Fig. 6 displays the pressure fluctuations over time at three distinct heights. As time progresses, intensive pressure fluctuations

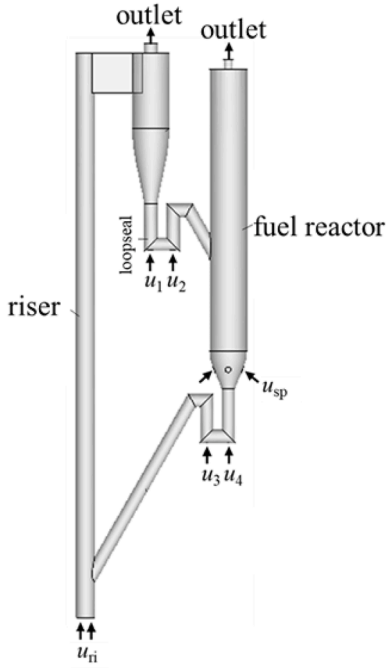

Fig. 2. Numerical structure of chemical looping hydrogen production system.

Table 2
Calculation parameters of CLHP. u_{riser} and u_{fr} represent gas inlet velocity for riser and fuel reactor, respectively. u_l is for the lower loop seal.

Name	Value	Unit
u_{riser}	5, 7, 9	m/s
u_{fr}	0.1, 0.3, 0.5	m/s
$u_{l,out}$	0.3, 0.5, 1.0	m/s
$u_{l,in}$	0.05, 0.3, 1.0	m/s
Particle diameter	150, 200, 250	μm
Particle density	2650	kg/m^3
Fuel	CO, CH_4, H_2	–
Temperature	1123, 1173, 1223	K
Pressure	1.0	atm
Calculation duration	60.0	*s*

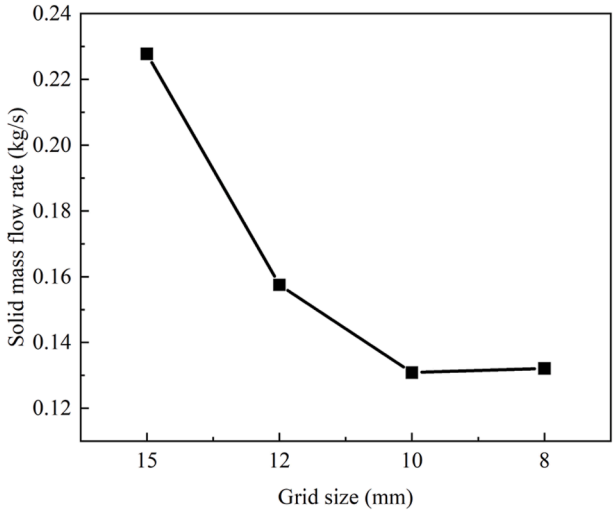

Fig. 3. Grid independence verification for chemical looping system.

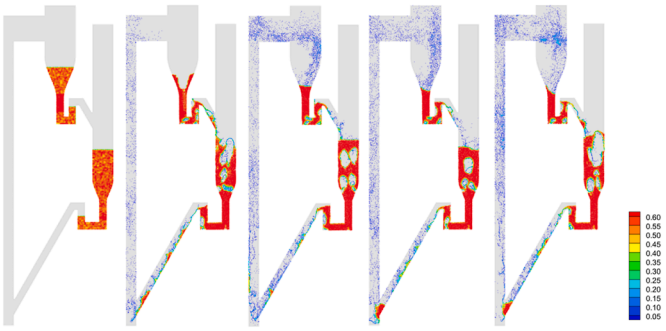

Fig. 4. Particle distribution at different time (0, 10, 20, 30 and 40 s).

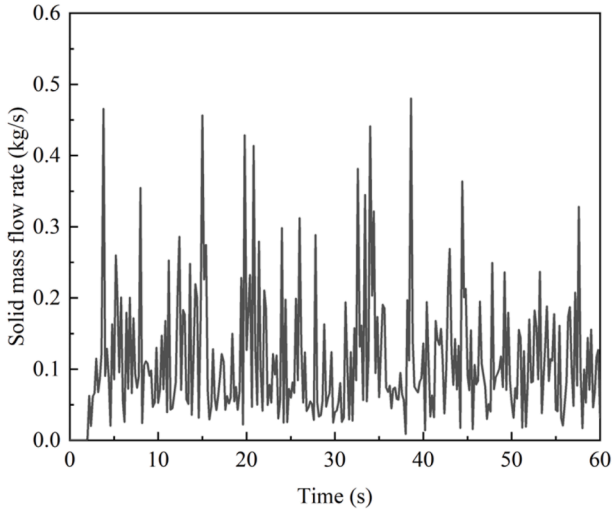

Fig. 5. Profile of solid circulation rate.

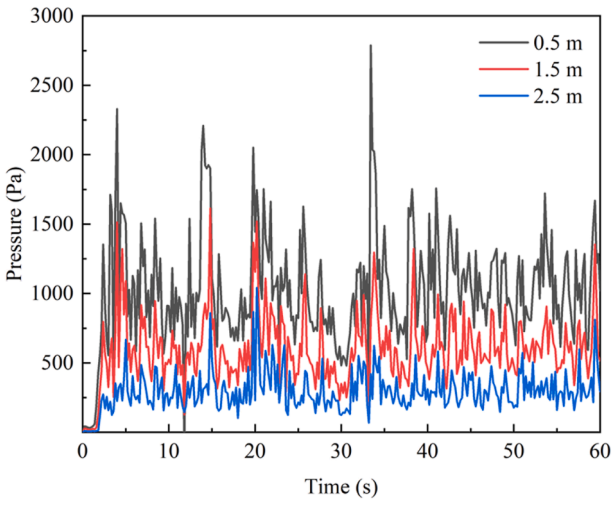

Fig. 6. Time-evolution of pressure at different heights.

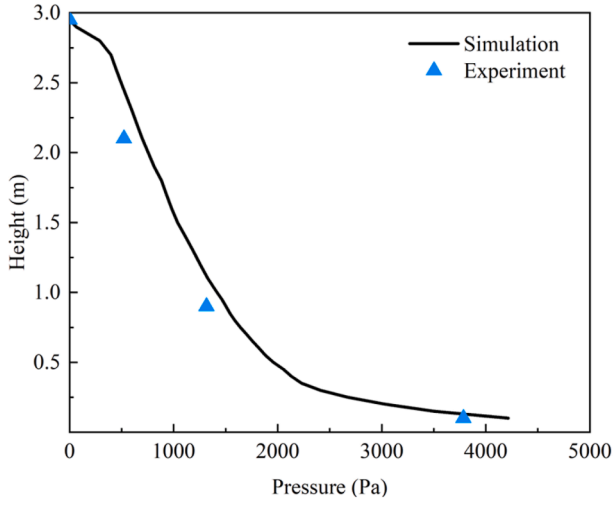

Fig. 7. Profile of time-averaged pressure distribution along height.

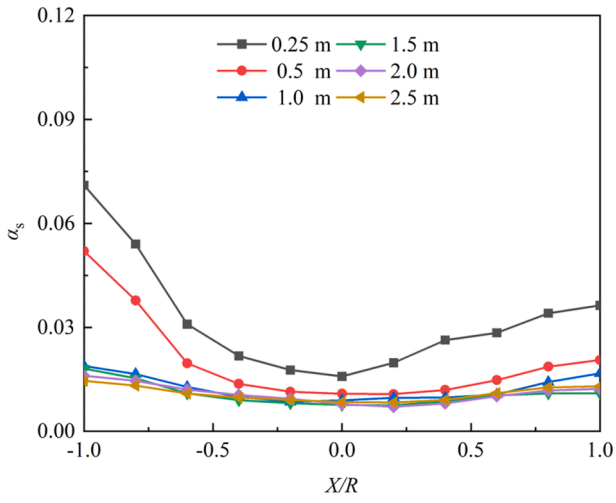

Fig. 8. Profile of radial distribution of time-averaged solid volume fraction at different height.

emerge. The amplitude and frequency of these fluctuations are directly linked to bubble dynamics, including bubble coalescence, breakup, and eruption at the bed surface. The formation and collapse of bubbles induce periodic pressure oscillations throughout the fluidized bed. Pressure signals at the lower height exhibit smaller but more regular oscillations due to the initial bubble generation near the distributor. The distinct temporal evolution of fluctuations indicates a transition from a steady-state bubbling regime to a more chaotic fluidization state, which may affect gas-solid contact efficiency. The data reveal that pressure decreases with increasing bed height.

Fig. 7 presents the axial profile of time-averaged pressure along the bed height. The time-averaged results distinctly demonstrate that pressure declines progressively with elevation. A steep pressure gradient occurs near the bottom region due to particle accumulation, while a gentler slope is observed in the middle-upper sections where particle density is lower. Triangular symbols denote experimental measurements in the figure. The computational results align closely with experimental data, validating the accuracy of the numerical methodology presented in this work.

Fig. 8 shows the distribution of solid volume fraction in riser at different heights. The distribution of volume fraction in riser is complex compared with fuel reactor and it exhibits a typical annular-core distribution pattern. Solid volume fraction is higher near the wall due to the friction between particle and wall. In the center, particles flow upwards together with gas. And solid volume fraction decreases with height. In the top region of riser, particle distribution tends to be consistent, approaching the patterns observed in pneumatic conveying.

3.2. *Influence of riser gas injection velocity*

The riser constitutes the most complex component in the current setup, with gas velocity representing one of the key factors influencing its operation. Three typical gas velocities (5, 7, and 9 m/s) were selected to investigate the influence of riser gas velocity on the chemical looping hydrogen generation process. Solid distribution in the riser, shown in Fig. 9, is dramatically influenced by the operating velocity of riser. When the riser injection velocity is 5 m/s, the distribution of solid is more like annular-core shape and the solid is dense near the wall due to the effect of wall. However, when velocity reaches 9 m/s, the distribution is near similar in radial direction. The effectiveness of gas transport is significantly greater than that of wall effects. Moreover, under low gas velocity conditions, the particle concentration decreases with increasing height, resulting in particle accumulation at the bottom. Conversely, under high gas velocity conditions, the particle concentration remains nearly constant along the riser height. This is more clearly observed in the pressure distribution profile, as shown in Fig. 10, where lower gas velocity results

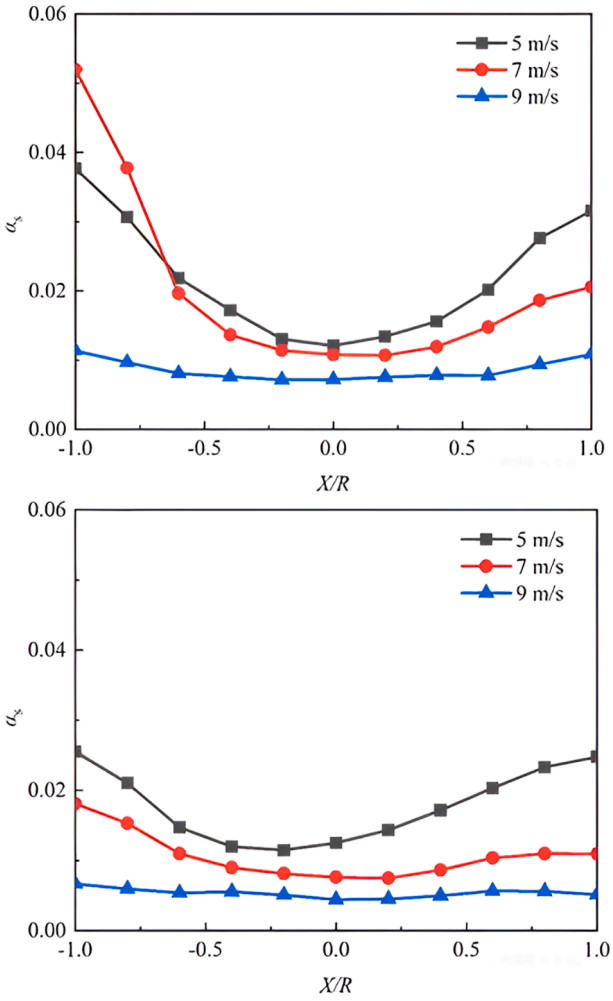

Fig. 9. Influence of riser gas velocity on the distribution of solid volume fraction in the riser. Up: $H = 0.25$ m. Bottom: $H = 1.5$ m.

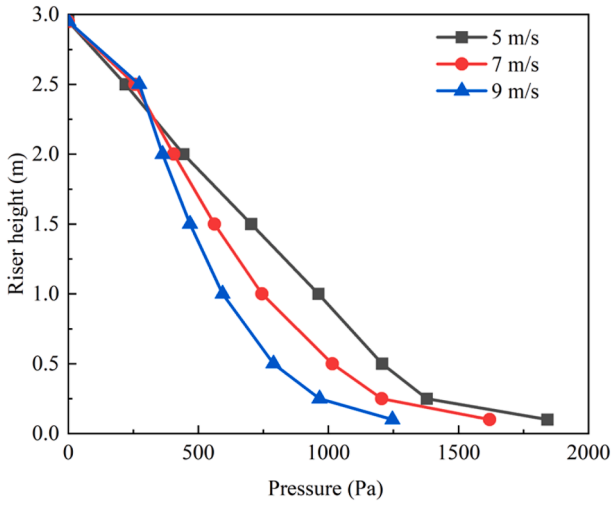

Fig. 10. Influence of riser gas velocity on the distribution of pressure in riser along height.

in greater particle accumulation at the bottom. These characteristics influence both the hydrogen production yield and efficiency in chemical looping hydrogen generation.

Fig. 11 shows the hydrogen generation under different riser gas velocity. The time-averaged hydrogen flow rate at the outlet decreases with increasing gas velocity, attributed to reduced solid-phase residence time leading to incomplete reactions. On the other hand, the hydrogen production per unit mass of oxygen carrier increases with gas velocity under current operating conditions.

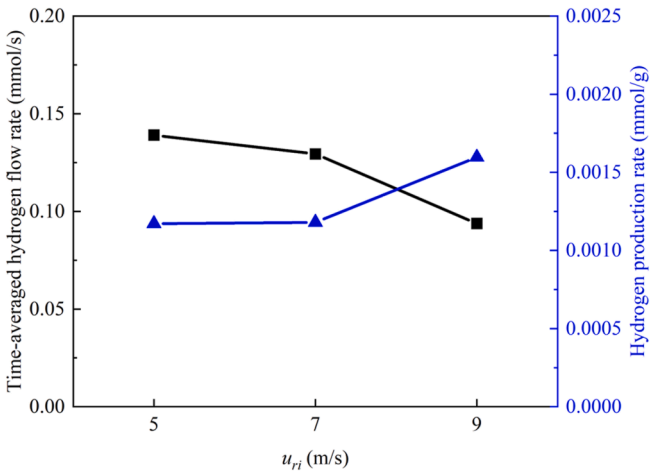

Fig. 11. Influence of riser gas velocity on the hydrogen production rate.

3.3. Influence of solid circulation rate

In chemical looping systems, the solid circulation rate directly determines the renewal rate of the oxygen carrier. An optimal circulation rate is essential to maintain reaction equilibrium and thermal balance. Higher circulation rates enhance gas-solid contact, shorten reaction time, and increase hydrogen production per unit time. Fig. 12 displays the pressure profiles under varying oxygen carrier circulation rates. Elevated circulation rates induce higher bottom pressure and more pronounced particle accumulation at the base. The increased total pressure drop in the riser indicates enhanced particle transport into the riser, where particles actively engage in hydrogen production reactions. As shown in Fig. 13, hydrogen yield rises with increasing solid circulation rates.

3.4. Influence of fuel flow rate

Fig. 14 presents particle flow behavior under varying fuel feeding rates. As shown, increasing gaseous fuel flow enlarges bubbles in the fuel reactor, altering fluidization dynamics. This modified gas-solid contact consequently changes fuel conversion. Correspondingly, Fig. 15 demonstrates that CO concentration at the fuel reactor outlet rises with higher fuel injection rates, while hydrogen in the fuel stream is fully converted throughout this process. Time-averaged hydrogen production data in Fig. 16 confirm enhanced hydrogen yield with increasing fuel supply.

3.5. Influence of particle property and temperature

The influence of operating temperature is shown and analysed in this section. As shown in Fig. 17, hydrogen flow rates were lowest at 1123 K but increased substantially to 1223 K. This marked upward trend stems from accelerated gas-solid reaction kinetics at elevated temperatures, which enhances both reduction and hydrogen production reactions, ultimately boosting hydrogen release. These results confirm the significant influence of temperature on hydrogen yield from oxygen carriers. Fig. 18 further compares time-averaged hydrogen production and hydrogen yield per unit mass of oxygen carrier across temperatures. Quantitatively, time-averaged hydrogen production rose from 0.09 mmol/s at 1123 K to 0.17 mmol/s at 1223 K (an 89% increase),

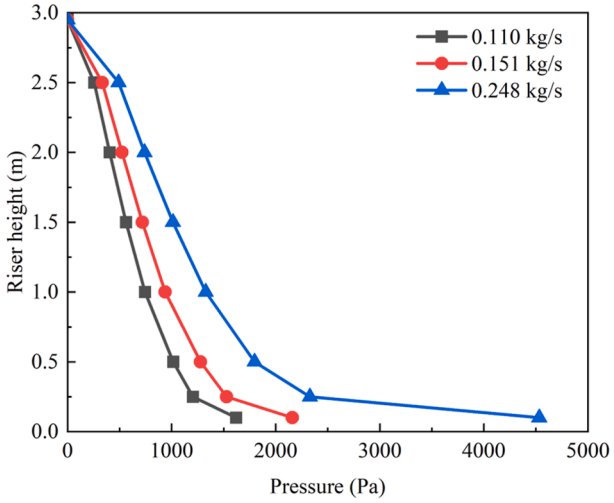

Fig. 12. Influence of solid circulating rate on the distribution of pressure in riser.

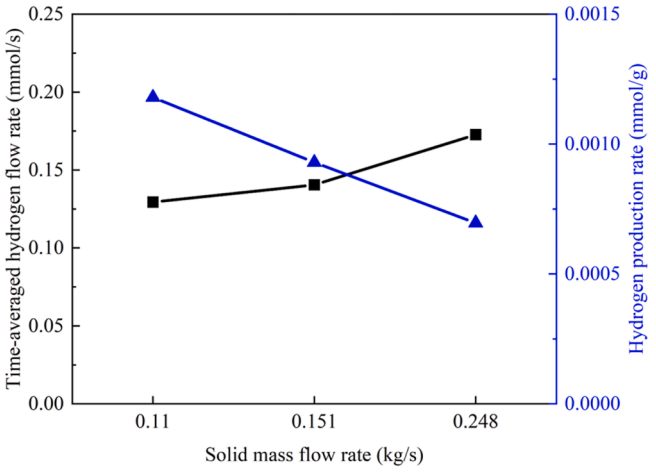

Fig. 13. Influence of solid circulating rate on the hydrogen production rate.

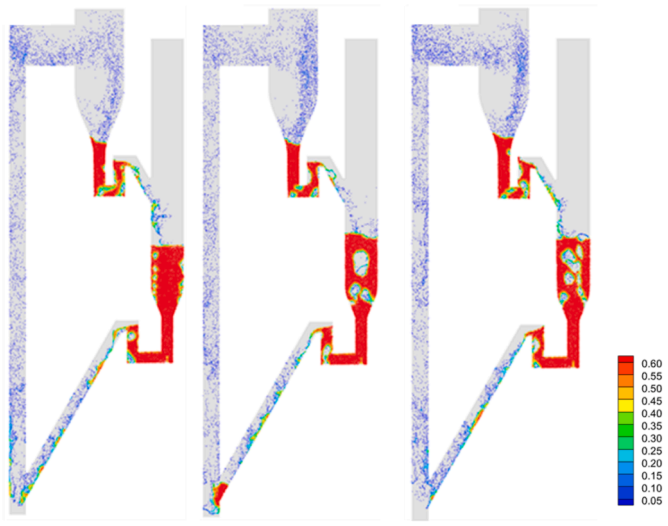

Fig. 14. Particle distribution under different fuel injection rate.

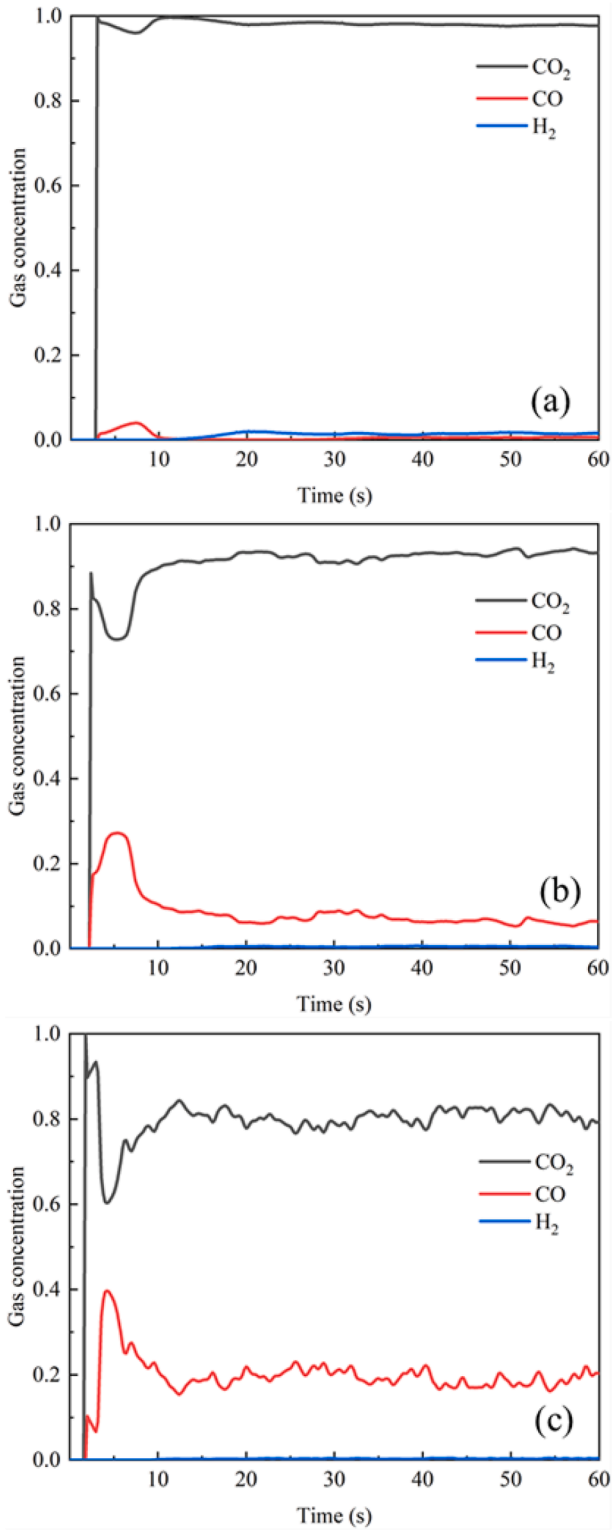

Fig. 15. Time-evolution of gaseous concentrations at outlet of fuel reactor.

while hydrogen yield per unit mass of oxygen carrier increased from 0.00078 mmol/g to 0.0014 mmol/g. This demonstrates that higher temperatures simultaneously improve total hydrogen output and oxygen carrier utilization efficiency, validating temperature's pivotal regulatory role in chemical looping hydrogen production performance.

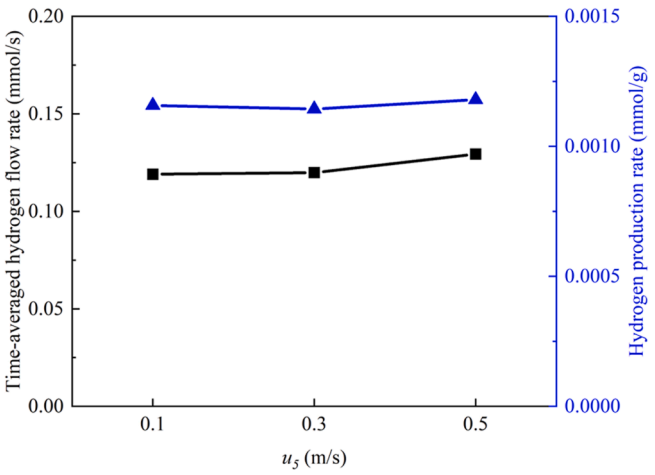

Fig. 16. Influence of fuel flow rate on the hydrogen production rate.

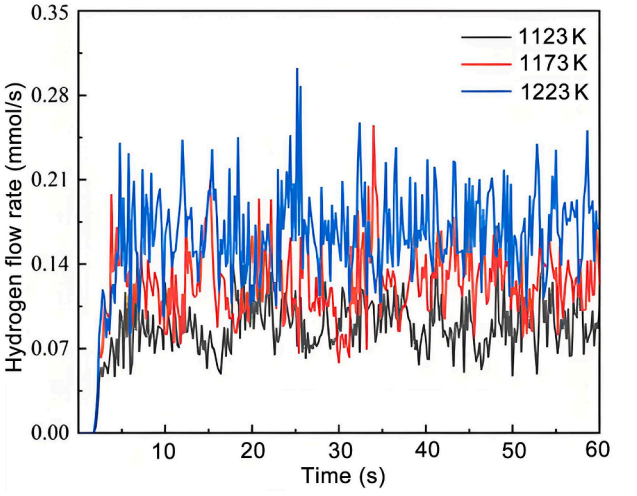

Fig. 17. Time-evolution of hydrogen production under different operating temperature.

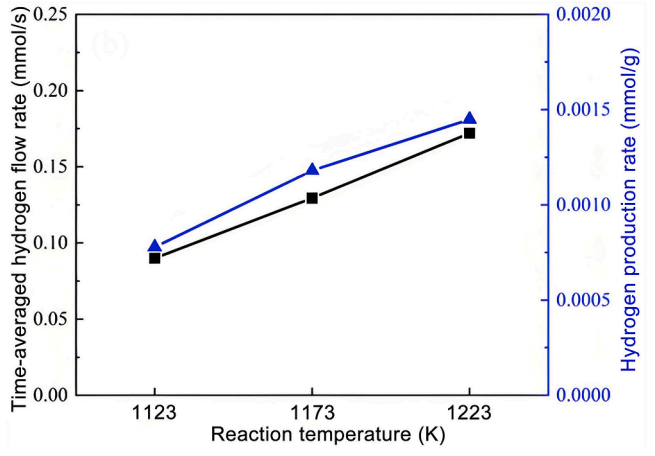

Fig. 18. Profile of time-averaged of hydrogen production under different operating temperature.

4. Conclusion

This study conducted a numerical simulation of a CLHP process by CPFD method. A fully-structured chemical looping reactor system was established, comprising a fuel reactor, a water splitting reactor, cyclone and loop seals. This system enabled the cyclic flow of oxygen carriers between reactors, demonstrating the complete process of CLHP. Simulations revealed the interaction mechanisms between reactors and the effects of localized perturbations on the overall system were analysed. Gas velocity in the hydrogen production reactor significantly influenced particle residence time and gas-solid contact duration. The solids circulation rate is a critical factor in chemical looping systems; increasing the circulation rate enhanced particle reaction within the riser, thereby increasing hydrogen production. Considering both hydrogen production yield and efficiency, a riser gas velocity of 7 m/s is recommended. Under the current conditions, temperature exhibited the most pronounced effect, with an approximate linear correlation observed, a 100 °C temperature increase yielded an approximately 50% rise in hydrogen production. And 1273 K corresponds to the highest hydrogen production yield. Overall, the design of CLHP systems requires primary focus on regulating the solid circulation rate and temperature. The findings will provide valuable guidance for the design and development of industrial-scale reactors.

CRediT authorship contribution statement

Liyan Sun: Writing – original draft, Validation, Methodology. **Yuedong Zhang:** Data curation, Methodology, Software. **Jialei Cao:** Methodology, Investigation, Formal analysis, Data curation. **Rui Xiao:** Writing – original draft, Supervision.

Declaration of competing interest

The authors declare that they have no known competing financial interests or personal relationships that could have appeared to influence the work reported in this paper.

Acknowledgement

This work is supported by National Key Research and Development Program of China (No. 2024YFE0208200). Authors also thank National Natural Science Foundation of China (No. 52336007), Fundamental Research Funds for the Central Universities (No. 3203002501C1, 2242025K30001), Xinjiang Key Laboratory of High Value Green Utilization of Low-rank Coal (Open Fund Project No. XJDX2314-ZD202401).

References

Abad, A., Adánez, J., Cuadrat, A., García-Labiano, F., Gayán, P., & de Diego, L. F. (2011). Kinetics of redox reactions of ilmenite for chemical-looping combustion. *Chemical Engineering Science, 66*(4), 689–702.

Abdullah, M. I., Fang, Y., Wu, X., Hu, M., Shao, J., Tao, Y., & Wang, H. (2024). Tackling activity-stability paradox of reconstructed niirox electrocatalysts by bridged w-o moiety. *Nature Communications, 15*, Article 10587.

Cao, H., Liu, M., Liu, L., & Xiang, D. (2024). Design, optimization, and technical evaluation of coking dry gas chemical looping hydrogen generation systems coupled with solid oxide fuel cell. *Applied Thermal Engineering, 239*, Article 122117.

Cao, J., Sun, L., Zeng, D., Yin, F., Gao, Z., & Xiao, R. (2024). Numerical simulation of chemical looping hydrogen generation with dual fluidized bed reactors. *CIESC Journal, 75*(8), 2865–2874.

Chen, X., Ma, J., Tian, X., Wan, J., & Zhao, H. (2019). Cpfd simulation and optimization of a 50 kwth dual circulating fluidized bed reactor for chemical looping combustion of coal. *International Journal of Greenhouse Gas Control, 90*, Article 102800.

Chen, K., Yuan, X., Tian, Z., Zou, M., Yuan, Y., Chen, Z., Zhang, Q., Zhang, Y. Y., Jin, X., Wu, T., Shahbazian-Yassar, R., & Liu, G. (2025). A facile approach for generating ordered oxygen vacancies in metal oxides. *Nature Materials, 24*, 835–842.

Chiesa, P., Lozza, G., Malandrino, A., Romano, M., & Piccolo, V. (2008). Three-reactors chemical looping process for hydrogen production. *International Journal of Hydrogen Energy, 33*(9), 2233–2245.

Chiesa, M., Mathiesen, V., Melheim, J. A., & Halvorsen, B. (2005). Numerical simulation of particulate flow by the eulerian–lagrangian and the eulerian–eulerian approach with application to a fluidized bed. *Computers & Chemical Engineering, 29*(2), 291–304.

Das, S., Biswas, A., Tiwary, C. S., & Paliwal, M. (2022). Hydrogen production using chemical looping technology: A review with emphasis on h2 yield of various oxygen carriers. *International Journal of Hydrogen Energy, 47*(66), 28322–28352.

Duan, C., Sun, Q., Zhu, X., Xu, M., Huang, Y., Xia, A., Zhu, X., & Liao, Q. (2025). Influence of potassium on the degradative solvent extraction process of biomass components cellulose, hemicelluloses and lignin. *International Journal of Biological Macromolecules, 304*, Article 140888.

Gao, Z., Wu, Di, Yin, F., Sun, L., Zeng, D., & Xiao, R. (2024). Thermodynamic and kinetic analysis on the biomass syngas fueled chemical looping hydrogen generation process in fixed bed reactor. *Energy, 298*, Article 131308.

Gupta, S., Choudhary, S., Kumar, S., & De, S. (2021). Large eddy simulation of biomass gasification in a bubbling fluidized bed based on the multiphase particle-in-cell method. *Renewable Energy, 163*, 1455–1466.

Hamidouche, Z., Ku, X., Lin, J., & Wang, J. (2020). Numerical simulation of a chemical looping combustion of biomass: Hydrodynamic investigation. *Fuel Processing Technology, 207*, Article 106486.

Hamidouche, Z., Masi, E., Fede, P., Simonin, O., Mayer, K., & Penthor, S. (2019). Unsteady three-dimensional theoretical model and numerical simulation of a 120-kw chemical looping combustion pilot plant. *Chemical Engineering Science, 193*, 102–119.

Jiang, H., Guo, H., Li, Y., Yang, H., Wang, C., & Lyu, J. (2024). Cpfd modeling of air-steam gasification of brewer's spent grains in a bubbling fluidized bed. *Fuel, 372*, Article 132132.

Jin, H., Wang, S., & He, Y. (2025). Investigation of drying process of non-spherical particle in a pulsed fluidized bed. *Particuology, 98*, 134–141.

Li, B., Wang, S., Yang, X., Wu, Q., & He, Y. (2020). Thermodynamic evaluation of sorption-enhanced chemical looping gasification with coal as fuel. *International Journal of Hydrogen Energy, 45*(41), 21186–21194.

Liu, Y., Chen, J., Ge, W., Wang, J., & Wang, W. (2011). Acceleration of cfd simulation of gas–solid flow by coupling macro-/meso-scale emms model. *Powder Technology, 212*(1), 289–295.

Prabhansu, D. S., Karmakar, M., Chandra, P., & Chatterjee, P. K. (2015). Studies on various drag models in fluidized bed forabatement of environmental pollution. *International Journal of Environmental Sciences, 5*, 1011–10321.

Snider, D. M., Clark, S. M., & O'Rourke, P. J. (2011). Eulerian–lagrangian method for three-dimensional thermal reacting flow with application to coal gasifiers. *Chemical Engineering Science, 66*(6), 1285–1295.

Sun, L., Masi, E., Simonin, O., Langørgen, Ø., Saanum, I., & Haugen, N. E. L. (2022). Three-dimensional unsteady numerical simulation of a 150 kwth full-loop chemical looping combustion pilot with biomass as fuel: A hydrodynamic investigation. *Chemical Engineering Science, 260*, Article 117835.

Sun, L., Xiao, R., Lin, J., Kong, D., Luo, K., & Fan, J. (2023). Numerical investigation of a 1mw full-loop chemical looping combustion unit with dual cfb reactors. *International Journal of Greenhouse Gas Control, 123*, Article 103835.

Uddin, M. B., Rasul, M. G., Ahmed Chowdhury, A., & Hassan, N. M. S. (2025). Hydrogen production from plastic waste pyrolysis syngas: A review on progresses and challenges. *International Journal of Hydrogen Energy, 158*, Article 150512.

Wang, I., Ji, G., Turap, Y., Nie, H., Li, Z., Zhao, M., & Wang, W. (2020). A short-cut chemical looping hydrogen generation system by using iron-based material from steel industry. *Chemical Engineering Journal, 394*, Article 124882.

Wang, S., Luo, K., Yang, S., Hu, C., & Fan, J. (2017). Parallel les-dem simulation of dense flows in fluidized beds. *Applied Thermal Engineering, 111*, 1523–1535.

Xue, Z., Chen, S., Wang, D., & Xiang, W. (2012). Design and fluid dynamic analysis of a three-fluidized-bed reactor system for chemical-looping hydrogen generation. *Industrial & Engineering Chemistry Research, 51*(11), 4267–4278.

Yin, F., Sun, L., & Xiao, R. (2025). Hydrogen generation via chemical looping water splitting over modified pyrite cinder as oxygen carrier fueled by biomass pyrolysis gas. *Chemical Engineering Journal, 507*, Article 159850.

Yin, L., Wang, S., Lu, H., Shuai, W., Pengfei, X., Lixing, W., & Yurong, H. (2010). Flow of gas and particles in a bubbling fluidized bed with a filtered two-fluid model. *Chemical Engineering Science, 65*(9), 2664–2679.

Zhang, J., Cai, Z., Shi, B., Ding, L., & Wang, Y. (2025). Mg–al spinel supported fe–zr oxygen carriers for chemical looping hydrogen generation at low temperatures. *International Journal of Hydrogen Energy, 158*, Article 150419.

Zhang, H., Zhu, A., Xu, J., & Ge, W. (2024). Gas–solid reactor optimization based on emms-dpm simulation and machine learning. *Particuology, 89*, 131–143.

Zhao, L., Dou, B., Zhang, H., & Wang, Z. (2021). Oxygen carriers for chemical-looping water splitting to hydrogen production: A critical review. *Carbon Capture Science & Technology, 1*, Article 100006.

Zhu, L., Zhao, Z., Liu, C., Zhang, Y., Zhang, Y., Zheng, C., Luo, K., & Xiang, G. (2023). Cfd-dem simulations of a gas-solid-liquid fluidization system: Effects on the flow field and particle behavior of semi-dry desulfurization fluidized bed. *Journal of Environmental Chemical Engineering, 11*(3), Article 109973.